

Chaos beyond linearized stability analysis: folding of the phase space and distribution of Lyapunov exponents

P. G. Silvestrov ^{a,b} and I. V. Ponomarev ^{c,d}

^a*Instituut-Lorentz, Universiteit Leiden, P.O. Box 9506, 2300 RA Leiden, The Netherlands*

^b*Theoretische Physik III, Ruhr-Universitt Bochum, 44780 Bochum, Germany*

^c*Naval Research Lab, Washington, DC 20375, USA*

^d*Queens College of the City University of New York, Flushing, NY 11367, USA*

Abstract

We consider a mechanism for area preserving Hamiltonian systems which leads to the enhanced probability, $P(\lambda, t)$, to find small values of the finite time Lyapunov exponent, λ . In our investigation of chaotic dynamical systems we go beyond the linearized stability analysis of nearby divergent trajectories and consider folding of the phase space in the course of chaotic evolution. We show that the spectrum of the Lyapunov exponents $F(\lambda) = \lim_{t \rightarrow \infty} t^{-1} \ln P(\lambda, t)$ at the origin has a finite value $F(0) = -\tilde{\lambda}$ and a slope $F'(0) \leq 1$. This means that all negative moments of the distribution $\langle e^{-m\lambda t} \rangle$ are saturated by rare events with $\lambda \rightarrow 0$. Extensive numerical simulations confirm our findings.

Key words: Lyapunov exponent, chaos, phase space bending

PACS: 05.45.-a, 05.45.Ac, 02.70.Rr

An exponential divergency of nearby trajectories in phase space is commonly considered as a paradigm of classical chaos [1,2]. The time evolution of the distance between two trajectories is determined by the stability matrix $\mathcal{M}(t)$, whose largest eigenvalue grows exponentially like $e^{\lambda t}$. For finite time t the value of λ depends on initial conditions and it is called a finite time Lyapunov exponent. The probability distribution of finite time Lyapunov exponents $P(\lambda, t)$ [2,3,4], especially its behavior at small λ , is important for many applications, where the measured quantity is sensitive to the existence of trajectories staying close for anomalously long time. Examples range from the problems of ocean acoustics [5] and branching of 2d electron flow [6] to Loschmidt echo [7] and mesoscopic superconductivity [8].

An evolution of small areas in phase space in the linearized approximation is described by a combination of area preserving stretching and squeezing (we assume two canonical variables x and p). In spite of a broad literature in the field the research which goes beyond the linearized stability analysis of dynamics of close trajectories is sparse. For dissipative systems it was done almost twenty years ago by Politi *et al.*[9] and by Ott *et al.*[10]. In those papers the authors considered the consequences of tangency between stable and unstable manifolds for chaotic attractors of nonhyperbolic two-dimensional maps. We are not aware that similar analysis was applied to the Hamiltonian systems. In this letter we try to fill this gap and consider the effect of bending of phase space on $P(\lambda, t)$ for area preserving systems. Although our approach is similar to the approach of refs. [9,10], their results were derived for the fractal dimension spectrum rather than for the finite time Lyapunov spectrum. Both characteristics are related to each other for dissipative systems (see Grassberger *et al.* in ref.[3]). However for Hamiltonian systems only the Lyapunov spectrum is meaningful. Its behavior at small λ , which is important for various practical applications [5,6,7,8], remains not covered in the existing literature.

As we will see, a creation of narrow folds in the course of mapping of the phase plane results in a great enhancement of the probability to find small values of λ . As a result all negative moments $\langle e^{-m\lambda t} \rangle$ for sufficiently large times are saturated by the rare events with $\lambda \rightarrow 0$.

For large times the probability distribution of finite-time Lyapunov exponents $P(\lambda, t)$ [2,3,4] has a generic form ($\lambda \geq 0$)

$$P(\lambda, t) \sim \exp [tF(\lambda)], \quad (1)$$

with a model specific function $F(\lambda)$ called spectrum [3]. The conventional selfaveraging Lyapunov exponent λ_0 appears in the expansion of spectrum around the maximum $F \approx -(\lambda - \lambda_0)^2 / 2\lambda_2$ (obviously $\langle \lambda \rangle = \lambda_0$, $\text{var} \lambda = \lambda_2 / t$ for $\lambda_0 t \gg 1$). If the evolution of the system is described by a Markovian process, i.e. if $P(\lambda, t)$ for large t is given by a convolution of $P(\lambda, t_i)$ for smaller time intervals, then naturally $F(0) = -\infty$. On the other hand, in case of mixed phase space one has $F(0) = 0$, due to the possibility for chaotic orbits to get "stuck" on the KAM tori [3,11]. In this letter we consider the distribution of Lyapunov exponents in the different regime of fully developed dynamical chaos (*i.e.* in the absence of stable periodic orbits). We argue that in this case the spectrum still has a finite limit $F(0) = \text{const} < 0$.

Dynamics of close trajectories is determined by the stability matrix via

$$\begin{pmatrix} \delta p \\ \delta x \end{pmatrix} = \mathcal{M} \begin{pmatrix} \delta p_0 \\ \delta x_0 \end{pmatrix}; \mathcal{M} = \begin{pmatrix} \frac{\partial p}{\partial p_0} & \frac{\partial p}{\partial x_0} \\ \frac{\partial x}{\partial p_0} & \frac{\partial x}{\partial x_0} \end{pmatrix}. \quad (2)$$

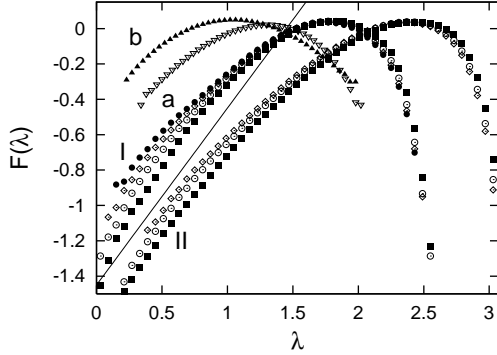


Fig. 1. The finite-time spectrum $F_t(\lambda)$ for the kicked rotator for different kicking strengths $K = 11$ (I) and $K = 20$ (II), and times $t = 10$ (■), 15 (○), 20 (◇), 25 (●), and for the time dependent random potential for two regimes a (▽) and b (▲) described in the text. In case b due to the small values of Lyapunov exponent both $F_t(\lambda)$ and λ were multiplied by 5. The solid line shows a slope $F'_t(\lambda) = 1$.

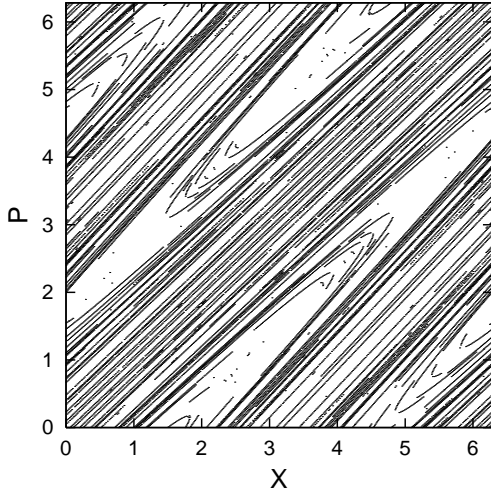


Fig. 2. Distribution of the endpoints of trajectories (x_t, p_t) having a small value of LE $\lambda < \lambda_0/18$, $\lambda_0 = \ln(K/2)$ for the kicked rotator with $K = 20$ after 5 iterations.

The finite time Lyapunov exponent, specific for a given trajectory, is defined as [12]

$$\lambda = (2t)^{-1} \ln \left[\text{tr} \mathcal{M}^T \mathcal{M} / 2 + \sqrt{(\text{tr} \mathcal{M}^T \mathcal{M} / 2)^2 - 1} \right]. \quad (3)$$

Before presenting the analytical theory, we show in Fig. 1 the function $F_t(\lambda) = \ln(P(\lambda, t))/t$, found numerically for two models. The first model, which we will primarily use, is the kicked rotator [1]:

$$p_{n+1} = p_n + K \sin x_n, \quad x_{n+1} = x_n + p_{n+1}. \quad (4)$$

The spectrum $F(\lambda)$ in Eq. (1) is strictly defined in the limit $t \rightarrow \infty$. Due to $\lambda \geq 0$, its finite time approximations $F_t(\lambda)$ always have $F_t(0) = -\infty$, but this singularity becomes weaker as time increases. This tendency can be observed

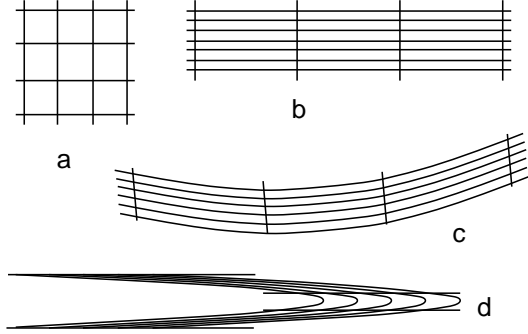


Fig. 3. Schematic presentation of the evolution of a small phase space area, described in the text.

in Fig. 1, where different finite time plots are presented (see especially the case for $K = 11$). Data on the figure includes $\sim 10^{12}$ trajectories. Calculation of the spectrum for longer times would require the unrealistic increase of the statistics. However the exponential divergency of close trajectories is already very noticeable, being $\delta x(t)/\delta x(0) \approx e^{45}$ for largest times in Fig. 1.

The second model describes a particle moving under the action of a time dependent random force, which we introduced via the “random kick” Hamiltonian

$$H = \frac{p^2}{2} + \kappa \sum_n \delta(t - n) \sum_{q=1}^N (a_q^{(n)} \sin qx + b_q^{(n)} \cos qx) \quad (5)$$

with random coefficients $|a_q^{(n)}|, |b_q^{(n)}| < 1$. Both plots in Fig. 1 are for $\kappa = 1$: the plot (a) has $N = 3$ and 50 random kicks, while the plot (b) has $N = 1$ and 300 kicks. The behavior of the spectrum for large λ is completely different for the two models. However, a shape of $F(\lambda)$ at small λ appears to be surprisingly similar. The results of all simulations are consistent with a linear increase at $\lambda \ll \lambda_0$, i.e. $F(0) = \text{const}, F'(0) = 1$.

The distribution of finite time Lyapunov exponents, Eq. (1), is a rough statistical characteristic which ignores correlations of values of λ between different trajectories. Such correlations are seen in Fig. 2, where we show the endpoints of trajectories, which have a small λ . The points on the phase plane are not distributed uniformly, as it would be for a random process, but form a pattern of narrow curved lines. Such a structure can be explained by the mechanism, schematically presented in Fig. 3. The figure shows a time evolution of small area of the phase plane around some classical trajectory $\{x(\tau), p(\tau)\}$. This evolution can be conveniently described by the transformation of a small piece of square lattice covering the area (Fig. 3a). Few stages of such an evolution are shown. (Estimates, analogous to that of Eqs. (6-12) below, were used in Refs. [9,10] in order to describe the fractal dimension spectrum $f(\alpha)$ of chaotic attractor.)

The first stage, shown in Fig. 3b, consists of linear extension and squeezing.

After the appropriate orientation of coordinate frame ($x, p \rightarrow u, v$) it may be expressed as

$$u \rightarrow ue^{\lambda_0 t_1}, \quad v \rightarrow ve^{-\lambda_0 t_1}. \quad (6)$$

At this moment we ignore the fluctuations of the Lyapunov exponents and use λ_0 for estimates. The linear transformation (6) always describes the evolution of infinitesimally small areas. For small but finite regions of phase space a nonlinear term should be added to Eq. (6)

$$u \rightarrow u, \quad v \rightarrow v + u^2/2, \quad (7)$$

which is shown in Fig. 3c (the orientation of initial axes (a) is different for Figs. 3b,c and d). Parabolas in Fig. 3c have a curvature comparable to the size of the system, or the typical momentum, both assumed to be of order unity. A consequent evolution of the area consists of further stretching and squeezing. However, the map, built from straight lines and parabolas shown in Fig. 3c, is robust under this transformation. Squeezing of a parabola gives another, more narrow, parabola. It is shown in Fig. 3d and may be expressed as

$$u \rightarrow ue^{-\lambda_0 t_2}, \quad v \rightarrow ve^{\lambda_0 t_2}. \quad (8)$$

Since the orientation of unstable manifold changes by π along parabola, the squeezing always leads to diminishing of the exponential divergency in some region near the vertex of the parabola. Thus a stripe with small values of λ is formed along the centres of a set of narrow parabolas shown in Fig. 3d. The curves in Fig. 2 show these stripes of small λ . Combining together eqs. (6-8) we express new coordinates u and v through initial ones u_0 and v_0

$$u = u_0 e^{\lambda_0(t_1-t_2)}, \quad v = v_0 e^{\lambda_0(t_2-t_1)} + \frac{u_0^2}{2} e^{\lambda_0(t_2+2t_1)}. \quad (9)$$

Now the Lyapunov exponent is calculated with the help of the stability matrix \mathcal{M} via $\lambda \approx \ln \mathcal{M}_{ij}^2/2t$ (3):

$$\lambda = \frac{1}{2t} \ln \left[2\text{ch}(2\lambda_0(t_1 - t_2)) + u^2 e^{2\lambda_0(t_2+t)} \right], \quad (10)$$

where $t = t_1 + t_2$. Thus the finite time Lyapunov exponent depends only on one variable u . The function $\lambda(u)$ (10) has a narrow minimum with the depth $\lambda_{min} = \lambda_0|t_1 - t_2|/t$, and the width $\delta u = \exp(\lambda_0(|t_1 - t_2| - t - t_2))$. This explains the pattern seen in Fig. 2. Away from the minimum we write

$$\lambda = \lambda_0 + (\ln |u| + \lambda_0 t_2)/t \quad \text{or} \quad |u| = e^{(\lambda - \lambda_0)t - \lambda_0 t_2}. \quad (11)$$

We see that at the time t small values of λ are found in narrow stripes on the x, p plane, each corresponding to the set of a squeezed parabolas (Fig. 3d). Among these lines those created at $t_1 \approx t/2$ have values as small as $\lambda \approx 1/t$, leading to nonvanishing $P(\lambda, t)$ at the origin: $F(0) > -\infty$. In order to estimate the probability distribution $P(\lambda, t)$ at $\lambda \ll \lambda_0$, we first notice that a fold

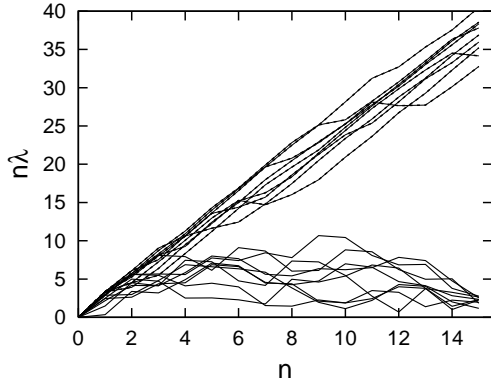


Fig. 4. $n\lambda$ versus n for kicked rotator with $K = 20$. Examples of typical trajectories (slope $\approx \ln(K/2)$, shown dashed), and rare trajectories having $\lambda \leq 1/5$ after 15 iterations (shown by solid lines).

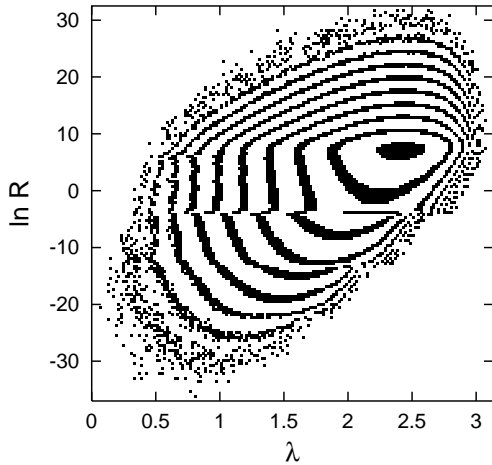


Fig. 5. The contour plot of the joint distribution $W(\lambda, \ln R)$ of the Lyapunov exponent and the logarithm of curvature, Eq. (19), for the kicked rotator with $K = 20$ after 15 iterations. Contours were drawn by taking 10^{12} initial conditions and allocating the results into the bins of two-dimensional histogram. The number of counts increases by 10 for each black contour, from outer to inner (the probability on the inner border of the contour is twice the probability on the outer side). The correlation between small λ and small R confirms our phase-space-folding induced mechanism.

created at time t_1 had a length ~ 1 . It becomes as long as $e^{\lambda_0 t_2}$ at the time t . Since the probability to find the Lyapunov exponent in the interval $d\lambda$ is given by the area, where such Lyapunov exponents are found, we may write

$$P(\lambda, t) \sim e^{\lambda_0 t_2} du/d\lambda \sim \exp[(\lambda - \lambda_0)t]. \quad (12)$$

We keep only exponentially large contributions in this estimate.

In derivation of (12) we ignored fluctuations of Lyapunov exponents during the squeezing stages (6) and (8). Due to fluctuations $P(\lambda, t)$ is saturated by

only exponentially small fraction of strongest folds. Still we may say that the simple folding mechanism described by the eqs. (6-9) is sufficient for having a finite value of the spectrum at the origin $F(0) > -\infty$. It is also capable to prevent the probability from decaying at small λ faster than $P(\lambda, t) \propto e^{\lambda t}$. Thus we write

$$F(0) = -\tilde{\lambda} \gtrsim -\lambda_0, \quad F'(0) \leq 1. \quad (13)$$

Taking into account fluctuations of the Lyapunov exponent during the stages (6) and (8) may be done as

$$P(\lambda, t) \sim \int e^{\lambda t - \lambda_1 t_1 - \lambda_2 t_2} P(\lambda_1, t_1) P(\lambda_2, t_2) \\ \times \delta(t_1 + t_2 - t) \delta(\lambda_1 t_1 - \lambda_2 t_2 - \lambda t) dt_1 dt_2 d\lambda_1 d\lambda_2. \quad (14)$$

Detailed investigation of this formula goes beyond the scope of this paper. The behavior $P(\lambda, t)$ at small λ may however be analyzed easily. One readily shows, that the spectrum of the form (13) with $F' \leq 0$ is consistent with the eq. (14). Substitution of $P(\lambda, t)$ in the form (13) into the r.h.s. of (14) leads to the same small λ behavior in the l.h.s. This does not happen for $F'(0) > 1$. Also if $F' \leq 0$, the integral over λ_1 and λ_2 for small λ is saturated by the region $\lambda_1, \lambda_2 \ll \lambda_0$. Figure 4 shows $n\lambda \sim \ln(\delta x_n / \delta x_0)$ for few typical trajectories and for the rare trajectories with anomalously small value of λ . As we see, typically two initially very close trajectories would escape from each other almost without fluctuations $\delta x(t) \sim e^{\lambda_0 t} \delta x(0)$. For rare trajectories, leading after large time t to $\lambda(t) \approx 0$, the extent of linear divergency is always much smaller, $\delta x(t') \ll e^{\lambda_0 t'} \delta x(0)$ for any $t' < t$, in agreement with (14).

Although our result eq. (13) gives only a bound on how fast the spectrum may increase with λ , $F'(0) \leq 1$, numerical simulations of Fig. 1 are consistent with $F'(0) \approx 1$. Even in this "weak" form the result (13) has a strong predictive power, leading to ($m = 1, 2, \dots$)

$$t^{-1} \lim_{t \rightarrow \infty} \ln \langle e^{-m\lambda t} \rangle = -\tilde{\lambda}. \quad (15)$$

The dominant contribution to the averaged value here comes from the rare trajectories with $e^{-\lambda t} \sim 1$. An exponentially small value of $\langle e^{-m\lambda t} \rangle$ is due to a small number of such trajectories. Eq. (15) should be compared with the often used Gaussian approximation $t^{-1} \ln \langle e^{-m\lambda t} \rangle_G \approx -m(\lambda_0 - m\lambda_2/2)$.

Folding of the phase plane requires an introduction of a new quantitative characteristic, in addition to Lyapunov exponent λ describing the linearized divergency of the trajectories. To describe folding we introduce the radius of curvature R of a small area bended in the course of evolution. To this end, we first analyze a *nonlinear* divergency of the closed trajectories by expanding the map (4) to the second order in the displacement between trajectories. If

we write two components of the displacement $\delta p, \delta x$ as a column \mathbf{q} , then

$$\mathbf{q}_n = \mathcal{M}_n \mathbf{q}_0 + \frac{1}{2} \begin{pmatrix} 1 \\ 0 \end{pmatrix} \mathbf{q}_0^T \mathcal{A}_n \mathbf{q}_0 + \frac{1}{2} \begin{pmatrix} 0 \\ 1 \end{pmatrix} \mathbf{q}_0^T \mathcal{B}_n \mathbf{q}_0, \quad (16)$$

where $\mathcal{M}_n, \mathcal{A}_n, \mathcal{B}_n$ are 2×2 matrices. The stability matrix for kicked rotator is given by a product

$$\mathcal{M}_n = \prod_{i < n} \begin{pmatrix} 1 & K \cos x_i \\ 1 & 1 + K \cos x_i \end{pmatrix}. \quad (17)$$

Two other symmetric matrices may be found from the recursion relations [13].

$$\begin{aligned} \mathcal{A}_{n+1} &= \mathcal{A}_n + (1 + K \cos x_n) \mathcal{B}_n - K \sin x_n \mathcal{C}_n, \\ \mathcal{B}_{n+1} &= \mathcal{A}_{n+1} + \mathcal{B}_n, \end{aligned} \quad (18)$$

where $\mathcal{A}_1 = \mathcal{B}_1 = 0$ and the elements of the matrix \mathcal{C}_n are $(\mathcal{C}_n)_{ij} = (\mathcal{M}_n)_{i2} (\mathcal{M}_n)_{j2}$. Consider the radius of curvature R of the image of a line $\mathbf{q}_0^T \equiv (0, \delta x)$ as a measure of bending (similar results may be obtained for the curvature of the image of line $\mathbf{q}_0 \equiv (\delta p, 0)$). A simple calculation gives

$$\frac{1}{R} = \frac{(\mathcal{A}_n)_{22} (\mathcal{M}_n)_{22} - (\mathcal{B}_n)_{22} (\mathcal{M}_n)_{12}}{((\mathcal{M}_n)_{12}^2 + (\mathcal{M}_n)_{22}^2)^{3/2}}. \quad (19)$$

In order to analyze correlations between folding and the values of the finite time Lyapunov exponent we introduce the joint distribution $W(\lambda, \ln R)$. It is shown in Fig. 5 [14]. We see that for given λ the curvature may vary by orders of magnitude. However the general trend is transparent: the smaller values of λ correspond to the smaller R [15].

The finite fraction of trajectories with $\lambda \approx 0$ in our mechanism does not require the existence of any stable islands. Still our main result (13) includes also the case of mixed phase space, corresponding to $\tilde{\lambda} = 0$. In the presence of very small stable islands one expects a competition of two effects, when our mechanism will govern the small λ spectrum at intermediate times, while the limit $t \rightarrow \infty$ will be due to dynamical traps [11] in the mixed phase space.

In conclusion, for the case of developed chaos, the physical quantities which may be calculated or measured naturally have a statistical meaning. In this letter we have shown, how in such systems folding of the x, p -plane inevitably leads to creation of elongated areas, where initially diverging trajectories revert to approaching to each other again. This allowed us to find a uniform description of the tail of distribution of finite time Lyapunov exponents, and to calculate all the negative moments of the distribution (15). Negative here

means that we are able to describe the physical quantities which are sensitive to the contributions where, in spite of chaos, trajectories stay longer together and do not diverge.

One immediate application of our findings will be a calculation of the Loschmidt echo [7], which was shown [16] to decay on average like $\langle e^{-\lambda t} \rangle$. This behavior should now be reconsidered in view of our eq. (15). Another problem of current interest, where the result is sensitive to the existence of long trajectories with small λ , is a calculation of the gap in the spectrum of the Andreev billiard [8]. Application of our result Eq. (13) to this problem leads to the strong modification of the low energy Andreev spectrum and substantial lowering of the superconducting gap [17].

Discussions with C. W. J. Beenakker, A. N. Morozov, J. Tworzydło, and J. Whitaker are greatly appreciated. This work was supported by the Dutch Science Foundation NWO/FOM and by the SFB TR 12.

References

- [1] B.V. Chirikov, Phys. Rep. **52**, 264 (1979).
- [2] E. Ott, *Chaos in Dynamical Systems* (Cambridge University Press, Cambridge, 1993).
- [3] P. Grassberger, R. Badii, and A. Politi, J. Stat. Phys. **51**, 135 (1988); M.A. Sepúlveda, R. Badii, and E. Pollak, Phys. Rev. Lett. **63**, 1226 (1989); J. Bene, P. Szépfalussy, A. Fülöp, Phys. Rev. A **40**, 6719 (1989)
- [4] H. Fujisaka, Prog. Theor. Phys. **70**, 1264 (1983); P. Grassberger and I. Procaccia, Physica D **13**, 34 (1984); R. Badii and A. Politi, Phys. Rev. A **35**, 1288 (1987); T. Tél, Phys. Rev. A **36**, 2507 (1987); H. Kantz and P. Grassberger, Phys. Lett. A **123**, 437 (1987); S. Vaienti, J. Stat. Phys. **56**, 403 (1989); F.J. Romeiras *et. al.*, Phys. Rev. A **41**, 784 (1990); B. Eckhardt and D. Yao, Physica D **65**, 100 (1993); C. Amitrano and R.S. Berry, Phys. Rev. E **47**, 3158 (1993); M.H. Ernst *et. al.*, Phys. Rev. Lett. **74**, 4416 (1995); A. Adrover and M. Giona, Physica A **253**, 143 (1998); A. Prasad and R. Ramaswamy, Phys. Rev. E **60**, 2761 (1999); F.K. Diakonov *et. al.*, Phys. Rev. E **62**, 4413 (2000); H. Yamada and T. Okabe, Phys. Rev. E **63**, 026203 (2001), H. Schomerus and M. Titov, Phys. Rev. E **66**, 066207 (2002); J. Szezech, S. Lopes, and R. Viana, Phys. Lett. A **335**, 394 (2005).
- [5] M.G. Brown *et. al.*, J. Acoust. Soc. Am. **113**, 2533 (2003).
- [6] M.A. Topinka *et. al.*, Nature **410**, 183 (2001).
- [7] R.A. Jalabert and H.M. Pastawski, Phys. Rev. Lett. **86**, 2490 (2001).

- [8] P.G. Silvestrov, M.C. Goorden, and C.W.J. Beenakker, Phys. Rev. Lett. **90**, 116801 (2003); M.G. Vavilov and A.I. Larkin, Phys. Rev. B **67**, 115335 (2003); C.W.J. Beenakker, Lect. Notes Phys. **667**, 131 (2005).
- [9] A. Politi, R. Badii, and P. Grassberger, J. Phys. A: Math. Gen. **21**, L763 (1988).
- [10] E. Ott, C. Grebogi, and J.A. Yorke, Phys. Lett. A **135**, 343 (1989).
- [11] G.M. Zaslavsky, Physica D, **168**, 292 (2002); M.F. Shlesinger, *et. al.*, Nature **363**, 31 (1993).
- [12] The matrix \mathcal{M} may be decomposed as $\mathcal{M} = \mathcal{U}\mathcal{T}$, where a real symmetric matrix \mathcal{T} ($\det \mathcal{T} \equiv 1$) describe squeezing and stretching with respect to some normal axes, and a normal matrix \mathcal{U} describes the rotation of the plane. We define λ (3) through the eigenvalue of $\mathcal{M}^T \mathcal{M} = \mathcal{T}^T \mathcal{T}$.
- [13] Solutions of eqs. (17,18) at each time step n comply with the conditions, imposed by the area conservation: $\det \mathcal{M} \equiv 1$, $\mathcal{M}_{11}\mathcal{B}_{11} + \mathcal{M}_{22}\mathcal{A}_{12} - \mathcal{M}_{12}\mathcal{B}_{12} - \mathcal{M}_{21}\mathcal{A}_{11} \equiv 0$, and $\mathcal{M}_{11}\mathcal{B}_{12} + \mathcal{M}_{22}\mathcal{A}_{22} - \mathcal{M}_{12}\mathcal{B}_{22} - \mathcal{M}_{21}\mathcal{A}_{12} \equiv 0$.
- [14] The distribution $W(\lambda, \ln R)$ has a main peak at $R \sim K^2$ and $\lambda \approx \ln(K/2)$. Second narrow peak at $R \sim 1/K$ corresponds to a minimal curvature which can be found from (19) after a single iteration of the map (4).
- [15] This distribution differs drastically from what we find for the mixed phase space. Mixed phase space takes place in the same model (4), but with smaller values of K ($K \lesssim 7$). In this case we found an extra pronounced maximum of $W(\lambda, \ln R)$ at small λ and $R \approx 1$. Moreover, even the exponentially small stability islands, which are hard to observe via the Poincare section, modify significantly the bivariate distribution $W(\lambda, \ln R)$.
- [16] P.G. Silvestrov, J. Tworzydło, and C.W.J. Beenakker, Phys. Rev. E **67**, 025204(R) (2003).
- [17] P.G. Silvestrov, Phys. Rev. Lett. **97**, 067004 (2006).